Arsenic (III) Detection with Underpotential Deposition and Anodic Stripping Voltammetry

Yifei Zhang, Dr. Danlei Li and Prof. Dr. Richard G. Compton*

Department of Chemistry, Physical and Theoretical Chemistry Laboratory, Oxford University, South Parks Road, Oxford, OX1 3QZ, UK

*Corresponding Author

Prof. Dr. Richard G. Compton, E-mail: Richard.compton@chem.ox.ac.uk

Abstract:

We report a stripping voltammetric method for the detection of aqueous As(III) using a Pt macroelectrode or a Pt nanoparticle-modified glassy carbon electrode (GCE) which, novelly, is based on the underpotential deposition of As atoms. The method consists of a pre-concentration reductive step to accumulate As ad-atoms onto Pt, followed by linear sweep voltammetry (LSV). It is shown that the stripping peak of As ad-atoms improves the response at low concentrations of As(III) as compared to analogous measurements using the deposition of bulk As. No interference was seen from Cu(II) at realistic concentrations although high concentrations of chloride inhibited the deposition of the ad-atoms. A linear response was found for the concentration range 0.05 to 1 µM As(III) at both types of electrode with a visually clear signal recorded at 0.05 µM (4 ppb), suggesting that this method has practical value noting the WHO limit of 0.13 µM (10 ppb) for safe drinking water.

Keywords: under-potential deposition; anodic stripping voltammetry; linear sweep voltammetry; arsenic; platinum nanoparticle.

Introduction:

Arsenic is highly toxic and exists both naturally and in some industrial or mineral effluents [1]. Long-term exposure to excess arsenic can cause severe health problems, including cardiovascular diseases, cancer and carcinogenic effects [1d, 1e]. The dominant inorganic arsenic species are As(-III) (as formally in AsH_3), As(0), As(III), and As(V). The latter two oxidation states are the major forms found in water [1a-c]. As(III) species (notably H_3AsO_3) are much more toxic than As(V) (H_2AsO_4 or $HAsO_4^-$) resulting from their interaction with enzymes in the human body [1d, 1e, 2]. Thus, the convenient detection of As(III) in water is both urgent and necessary. The significant contamination of groundwater by arsenic has been found in over 20 countries [2], in which the arsenic levels are above the World Health Organization's (WHO) arsenic guideline value of 10 μg L^{-1} (10 ppb) in drinking water [3].

There have been many methods developed to determine arsenic levels in water during the past decades [4], including important techniques such as atomic absorption spectrometry (AAS) [5], inductively coupled plasma mass spectrometry (ICPMS) [6], and high-performance liquid chromatography with ICPMS (HPLC-ICPMS) [7]. However, these sensitive instrumental methods require dedicated laboratory conditions and have long sample preparation times. Therefore, alternative techniques that can overcome these problems need to be developed. Electrochemical methods can provide highly sensitive and rapid detection [1a, 8]. In particular stripping voltammetry is a powerful method for quantitative detection of low levels of analytes [9]. Many studies have reported using stripping voltammetry methods for detecting As(III) in aqueous solution, including anodic stripping voltammetry (ASV) at gold nanoparticle-modified GCE [10] or at a boron-doped diamond (BDD) electrode [11], and cathodic stripping voltammetry (CSV) at a hanging mercury drop electrode (HMDE)[12].

ASV is the most commonly used electrochemical method for As(III) detection in water. Simm *et al* used ASV to detect As(III) at Ag macroelectrode with a sensitivity of 2.6 A M^{-1} and reached a LOD of 13.5 ppb [13] whilst Bu *et al* investigated arsenic in water by linear sweep anodic stripping voltammetry

(LSASV) at Au macrodisk electrodes, and obtained a detection limit of 0.14 ppb for As(III) with a sensitivity of 761 A M^{-1} [14]. Using ASV, Dai *et al* found a LOD of 35 ppb for As(III) at a Pt macroelectrode [15]. To date, using conventional metal electrodes the lowest LOD of 0.003 ppb was reported by Profumo *et al* [16] and the greatest sensitivity of 1985 A M^{-1} was achieved by Xiao *et al* [10]. However, the detection of As(III) via ASV at conventional electrodes is subject to interferences by metal ions, including copper, lead, zinc, iron, silver, bismuth and mercury [1a]. The most commonly reported interfering ion is Cu^{2+}, which can alter the stripping peak of As [17]. This interference has been ascribed to the formation of intermetallic compounds or a Cu-As alloy together with the similar reduction potentials of Cu(II) and As(III) noted by Idris *et al* [18].

In recent years, nanomaterials have been incorporated into electrochemical methods for As(III) detection where claimed advantages include their high surface area, increased catalytic sites, and higher adsorption capacities [19]. In the context of ASV the high surface areas offer obvious advantages in providing scope for enhanced sensitivity whilst the different surface structures that can prevail at the nanoscale may offer possibilities for changing the metal deposition chemistry to avoid the interference effects noted above. Proof of concept that particle modified glassy carbon electrodes (GCEs) can be employed for the trace detection of As(III) using ASV has been reported in several works based on Pt nanoparticles [20]. Xiao *et al* studied Au nanoparticles modified carbon nanotubes (AuCNTs) on glassy carbon electrodes to detect As(III) in water via ASV [10]. The LOD was determined to be 0.1 ppb and the sensitivity was 1985 A M^{-1} via Square Wave ASV. The very high sensitivity was attributed to the high number of tiny Au nanoparticles supported on the large area of CNTs. The dramatically increased area can influence the voltammetric responses [21] in that the overpotential required for slow ('irreversible') electron transfer reactions can be lowered [22] whilst the magnitude of the flux of analyte to the electrochemical interface reflects the extent of the overlap of the diffusional fields of the different centres which is ultimately limited, in the case of full overlap, by diffusion to the full geometrical area of the supporting electrode.

Beyond ASV nanoparticle modified electrodes have been used for diffusional voltammetry. For example, Dai *et al* modified a glassy carbon electrode with Pt nanoparticles via electrodeposition to electrocatalytically oxidize As(III) to As(V), and reported an As(III) detection limit of 2.1 ppb [15] and a similar approach taken using Pt nanoparticles and CNTs [23] presented a LOD of 0.12 ppb. Huang *et al* used Au nanoparticles within a thin Nafion film to modify glassy carbon giving a sensitivity of 23.98 A M^{-1} and a low LOD of 0.047 ppb [24]. Yang *et al* used porous gold nanoparticles to modify glassy carbon electrodes giving a sensitivity 0.617 A M^{-1} cm^{-2} and a low LOD of 1.668 ppb [25] where the number of significant figures is that reported by the authors.

The sensitivity of diffusion signals are ultimately constrained by the rate of transport of redox species to the geometric area of the electrode used whilst stripping voltammetry, as discussed above, is subject to possible interference by species which form alloys and/or intermetallic species with As. Both types of measurements are well explored and optimised. In the present paper we adopt a different strategy based on ASV aiming to overcome the interference problem through avoiding the formation of *bulk* deposits of As or its alloys/compounds. In particular we consider the phenomenon of under potential deposition (UPD) as a possible means of avoiding such interference. This is the deposition (usually) of a metal in the form of a monolayer or sub-monolayer at potentials lower than those required to form the bulk material [12, 26]. The topic has been extensively investigated by surface electrochemists [27] but little used analytically [28]. In the present case we note that As undergoes UPD on Platinum surfaces [29]. Accordingly we investigate the possible use of this for the analysis of As at low concentrations via what we term 'UPD-ASV'. In order to ensure a sufficiently sensitive stripping signal we use a Pt nanoparticle-modified electrode to give a large area of Pt on which to deposit the As. Comparisons are made with measurements at bulk Pt using a Pt macrodisc electrode and the UPD-ASV approach was shown to be valuable particularly in avoiding interference caused by Cu(II). The measured detection limits using either a Pt macroelectrode or a Pt nanoparticle-modified electrode for As detection were within the requirements for the WHO limits for drinking water with visually distinct and recognisable signals seen at the lowest concentrations reported.

Table 1 compares methods developed for arsenic detection in this work with recent literature. Compared to previous work, our method is only interfered with by chloride at relatively high concentrations and interference by copper is avoided. In addition, the low limits of detection claimed in the literature on the basis of the 3σ method [30] contrasts with the values reported from measured voltammetric signals in this work.

Table 1. Summary of Different Methods Developed for Arsenic Detection

Authors	Electrode	Method	Interference ion	LOD / ppb
Bhanjana *et al* [31]	ZrO_2/Nafion-Au electrode	CV	No interfered ions	5
Yang *et al* [30a]	np-Au-GCE	SWASV	Humic acid, Pb^{2+}	0.137[1]
Sonkoue *et al* [30b]	AgNP-GCE	CV	Cu^{2+}	0.1[1]
Hwang *et al* [30c]	Fe/Chitosan-SPCE	SWASV	Cu^{2+}	1.12[1]
Nunez *et al* [30d]	Graphene-SPCE	DPAV	Cu^{2+}	0.28[1]
This work	Pt macroelectrode, Pt nanoparticle-modified GCE	ASV	Cl^- (higher than 100 µM)	4*, 4*

AuNP: gold nanoparticle; GCE: glassy carbon electrode; np: nanoporous; SPCE: screen-printed carbon electrode; CV: cyclic voltammetry; SWASV: square wave anodic stripping voltammetry; DPAV: differential pulse anodic voltammetry; ASV: anodic stripping voltammetry; LOD: limit of detection. [1] LOD calculated from the 3σ method. * LOD obtained from measured signals.

Experimental

Chemical reagents

Commercially available Pt nanoparticles (0.05 mg mL^{-1}, 30 nm in diameter, NanoComposix, USA) were dispersed in 2 mM sodium citrate. Sodium (meta) arsenite ($NaAsO_2$, 99%, Fluka, Switzerland), copper(II) sulfate pentahydrate ($CuSO_4 \cdot 5H_2O$, 99%, Sigma Aldrich, UK), potassium chloride (KCl, 99.5%, Sigma Aldrich, UK), and sulphuric acid (H_2SO_4, 98%, Fisher Scientific, UK) were purchased and used without any further purification. All aqueous solutions were prepared using deionized water (Milipore, UK) with a resistivity of 18.2 MΩ cm at 298 K.

Instrumentation

Electrochemical measurements were conducted with a standard three-electrode system in a Faraday cage at 298 (±0.1) K. A glassy carbon electrode (GCE, diameter of 3.00±0.01 mm, geometric area of 0.07 cm^2, BAS technical, UK) or a platinum macroelectrode (diameter of 1.66±0.01 mm, geometric area of 0.02 cm^2, BASi, USA) served as a working electrode, and a platinum wire was applied as a counter electrode with a mercury-mercurous sulfate reference electrode (MSE, BASi, USA). The solution used in the reference electrode was saturated K_2SO_4 solution (1.45 M) conferring the reference electrode with a potential of +0.65 V vs. standard hydrogen electrode (SHE). Electrochemical measurements were performed in 0.1 M H_2SO_4 containing various concentrations of As(III) and were recorded with a μAutolab type III potentiostat (EcoChemie, NL) after degassing with nitrogen.

Preparation and characterization of Pt nanoparticle-modified electrodes

The GC electrode was cleaned on polishing pad with alumina of decreasing particle sizes (1, 0.3 and 0.05 μm) then rinsed with deionized water. For drop casting Pt nanoparticles, 5 μL of stock Pt nanoparticle suspension was drop casted onto the GC electrode using micro pipette and dried with a gentle N_2 flow for 15 minutes.

As is shown in Figure 1a), the individual particles are formed by aggregation of much smaller nanoparticles of approximate 3 nm in diameter [32], which makes the particles exhibit a distinct porous structure. The particles are capped by citrate, and the real surface area of the mesoporous Pt nanoparticles were calculated to be 0.013 ± 0.003 μm^2 per particle from previous reports based on single entity electrochemistry [32].

According to the optical microscopy images shown in Figure 1b, a ring-like pattern was formed on the surface of electrode after the drop casting of Pt nanoparticles, so-called the coffee ring pattern [33]. It was previously characterized by SEM [34] and shown that although most of the particles are deposited as part of the 'ring' a few particles remain randomly distributed around the centre of the drop cast (Figure 1c) [34] but which is mostly empty of deposit. The average particle-particle distances even in the centre for the mass drop casted were shown to be sufficiently small so as to allow diffusional overlap so that analyte diffusion to the full geometric area of the electrode was observed [34].

Optical Microscopy and imaging

All images were obtained using an optical microscope, Zeiss Axio Examiner, A1 Epifluorescence microscope (Carl Zeiss Ltd., UK). The objective lens used was a 10× air objective (NA = 0.5, EC Plan-Neofluar) and the light source employed in this study was a LQ-HXP 120 V lamp. Incident light reaching the surface of the GCE was partly reflected to the camera through the objective lens and the image of the electrode was obtained by a black & white ORCA-Flash 4.0 digital CMOS camera (Hamamatsu, JP). The resolution of the image was 4-megapixel.

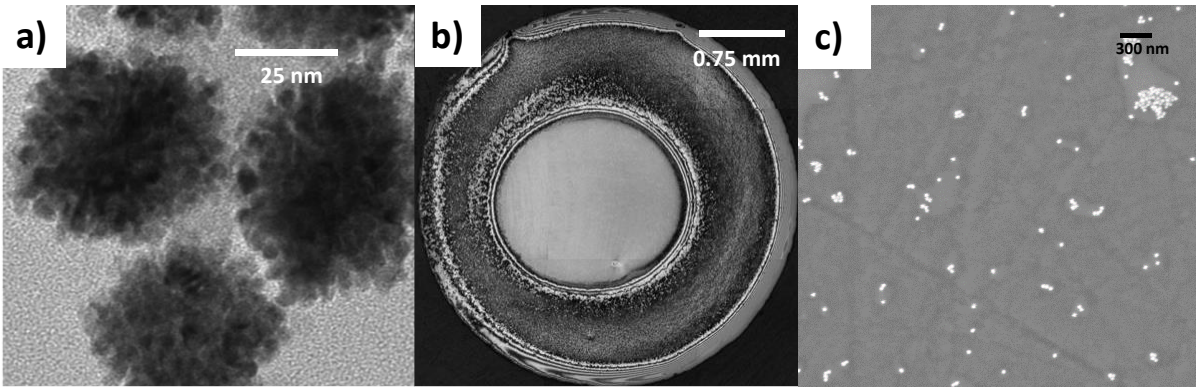

Figure 1. a) HR-CTEM image showing how the overall single nanoparticle structure comprises of an aggregate of smaller substituent crystallites. Reprinted with permission from Ref. [32]. Copyright (2019) Royal Society of Chemistry. b) Image of 0.25 µg of Pt nanoparticle drop casted onto a GC electrode. c) SEM images of the centre of the drop cast. Reprinted with permission from Ref. [34]. Copyright (2020) John Wiley & Sons, Inc. The diameter of the GC electrode was 3 mm and the geometric area of the GC electrode was 0.07 cm^2. The average number of particles was 1.6×10^{10} particles cm^{-2}. The diameter of the Pt nanoparticles is 30 nm and dispersed in 2 mM sodium citrate solution. The scale bar is 0.75 mm.

Results and discussion

In the following sections, first, the electrochemical behaviour of As(III) at both Pt macroelectrodes and Pt nanoparticle-modified electrodes were studied in solution containing 500 µM $NaAsO_2$ with 0.1 M H_2SO_4 using cyclic voltammetry. The voltammetric peaks were assigned and compared with literature. Next, methods for achieving a low limit of detection of As were investigated using anodic stripping voltammetry with the Pt surface pre-concentrated with As(0) either as bulk As or as ad-atoms formed by under potential deposition (UPD). The applied potential and duration for pre-concentration were optimised on the basis of higher signal-to-background ratio and the benefits of using UPD identified. Finally, attention is given to possible interferences.

Cyclic voltammetry of aqueous As(III) at bulk Pt and at Pt nanoparticles

To examine the electrochemical responses of As(III), a Pt macroelectrode and a Pt nanoparticle-modified GCE were first employed to study the behaviour of As(III) in solution containing 500 µM $NaAsO_2$ with 0.1 M H_2SO_4 using cyclic voltammetry as is shown in Figure 2 where the arrow stands for the starting direct of scan. Acidic conditions are used to avoid the formation of insoluble oxides. Figure 2a illustrates the cyclic voltammetric response of As(III) in 0.1 M H_2SO_4 with a potential window from -0.8 V to +0.9 V (vs. MSE) at 0.1 V s^{-1} at a Pt macroelectrode. Three peaks were observed on the cathodic scan, labelled as peak 1, peak 2 and peak 3 (solid line in Figure 2a). Peak 1 at ca -0.08 V was ascribed to the reduction of Pt-O to Pt [15, 29a]. Peak 2 observed at ca -0.6 V corresponds to the three-electron reduction of As(III) to As(0) [29a]. Peak 3 at ca -0.77 V represents the hydrogen evolution reaction (HER). On the reversal anodic scan, three peaks, peak 4, peak 5 and peak 6 were obtained. Peak 4 with the potential of ca -0.75 V represents the hydrogen oxidation reaction (HOR). Peak 5 at ca -0.25 V corresponds to the re-oxidation of As(0) to the parent As(III) species [29a]. A larger oxidation peak, peak 6, was observed at ca +0.4 V at which As(III) was further oxidized to As(V). Comparing with the voltammogram obtained in blank solution (0.1 M H_2SO_4; dashed line in Figure 2a), it can be seen that the three absent peaks (peak 2, peak 5 and peak 6) are all As(III)-related peaks, and peaks 3 and

4 correspond to HER and HOR, respectively [29a]. Peak 6' observed at ca +0.5 V in blank solution was assigned to be the oxidation of Pt to Pt-O [29a]; this corresponding Pt oxidation peak was immersed to As(III) oxidation peak (peak 6; solid line in Figure 2a) and hardly been distinguished when 500 µM As(III) was added in solution. On the other hand, similar peak current densities of peak 1 were observed in both blank solution and solution containing 500 µM As(III) due to the reduction of Pt-O to Pt in both cases[15, 29a].

The cyclic voltammetric response at a Pt nanoparticle-modified GCE with an average surface coverage of 2.2×10^{-14} mol cm^{-2} (ca 0.1 monolayers, calculations are shown in SI section 1) is shown in Figure 2b. The potential window of voltammogram was from -0.8 V to +0.9 V and the scan rate was 0.1 V s^{-1}. The voltammetry obtained in the absence of As(III) in 0.1 M H_2SO_4 at the Pt nanoparticle-modified GCE (dashed line in Figure 2b) was similar to the one measured at the Pt macroelectrode (dashed line in Figure 2a). All peaks were at similar potentials and represent the same electrochemical processes as discussed above. In 500 µM As(III) in 0.1 M H_2SO_4 (solid line in Figure 2b), as seen with Pt macroelectrode six voltammetric features were discerned and assigned to the same electrochemical reactions [15, 29a] as above. It was noted that peaks 3, 4, 5 and 6 had similar peak potentials (solid line in Figure 2b) to those seen at bulk Pt. However, peak 1 and peak 2 in Figure 2b differ from the ones in Figure 2a. It is clear that peak 1 only appeared after a full scan of CV at Pt macroelectrode (Figure 2a) while at Pt nanoparticle-modified GCE peak 1 was observed during the initial cathodic scan (Figure 2b). The absence of peak 1 during the initial cathodic scan on Pt macroelectrode suggests a near oxide-free Pt surface whilst the Pt nanoparticles deposited on GCE may contain Pt oxide on their surfaces which results in the appearance of peak 1 on the cathodic scan in Figure 2b. Furthermore, the peak potential of peak 1 at Pt nanoparticles at ca -0.2 V (Figure 2b) was more negative compared to the potential at bulk Pt (Figure 2a). This potential is similar to that reported by Postek *et al* in 2019 [20c] for Pt nanoparticles of size 4 to 7 nm and was assigned to the reduction of Pt oxide to Pt.

Peak 2 (Figure 2) was seen at ca -0.6 V for both Pt nanoparticle-modified electrode (solid line in Figure 2b)and Pt macroelectrode (solid line in Figure 2a), which corresponds to the reduction of As(III) to As(0) [15]. The relatively large current density of peak 2 at Pt nanoparticle-modified electrode is possibly due to the higher surface area and hence more deposition sites for As(0) on the mesoporous Pt nanoparticles, together with reduced interference from the solvent breakdown. Similarly peak 5 on the reverse anodic scan in Figure 2b is seen to be enhanced for the nanoparticles over the bulk Pt. However, from an analytical perspective the CV method typically does not provide a suitably low detection limit since this is limited by diffusion. Thus, a different method needs to be applied to approach a low detection limit. The next section focuses on the detection of As using anodic stripping voltammetry where a pre-concentration of As(0) was applied to enhance the signal and to approach a lower detection limit.

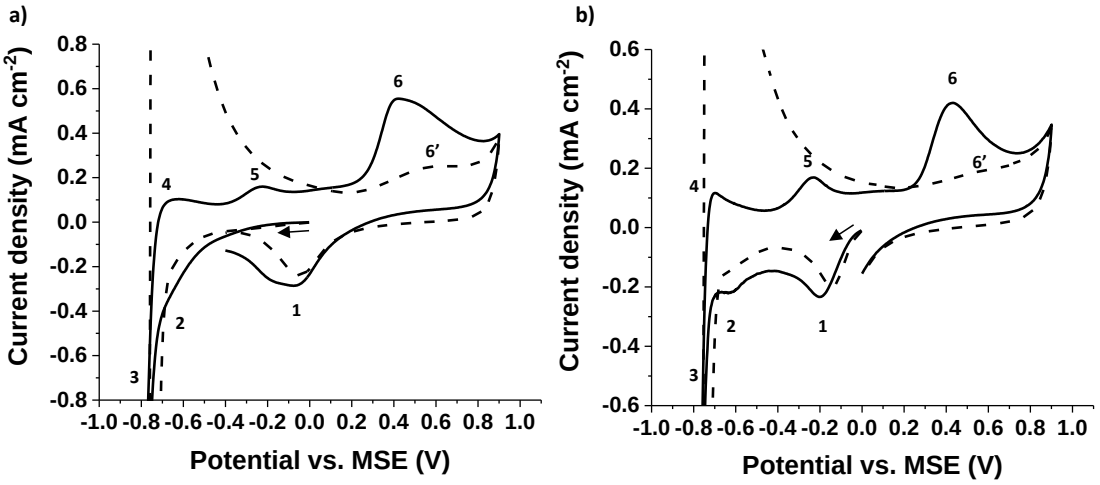

Figure 2. CV curves of a) 500 µM $NaAsO_2$ in 0.1 M H_2SO_4 (——) and blank (- - -) at Pt macroelectrode, and b) 500 µM $NaAsO_2$ in 0.1 M H_2SO_4 (——) and blank (- - -) at Pt nanoparticle-modified GC electrodes. The voltammograms were conducted from 0 V and first scanned cathodically to -0.80V at a scan rate of 0.1 V s^{-1} and then scanned anodically to +0.9 V. The current densities were calculated based on the geometric area of Pt macroelectrode, 0.02 cm^2 and estimated Pt nanoparticles surface area, 0.11 cm^2. Calculations of particles surface area are shown in the supporting information (SI) section 1. The arrows represent the starting point and the direction of scan.

Anodic stripping voltammetry of As(III) at bulk Pt and Pt nanoparticles

To examine the possibility of achieving a lower detection limit of As(III) in water, anodic stripping voltammetry was applied for the detection of As(III) in 0.1 M H_2SO_4 on both a Pt macroelectrode and Pt nanoparticle-modified GCEs. The pre-concentration of As(0) was first carried out at -0.7 V for 240 s

during which both bulk As(0) and As ad-atoms were deposited at the surface of Pt [29a]. Then the deposited As(0) was stripped off from the electrode surface using LSV conducted from -0.7 V to +0.9 V at a scan rate of 0.1 V s^{-1}. The deposition potential and time for ASV were optimized for the signal-to-background ratio and is given in SI sections 2 and 3, respectively.

The method of using UPD-ASV method to detect arsenic is shown schematically in Scheme 1. For Pt macroelectrodes, As(III) was reduced to As(0) and As atoms deposited onto the surface of Pt during pre-concentration. When a anodic potential sweep was applied to the electrode, As(0) ad-atoms were stripped off and oxidized to As(III) and a stripping peak was obtained from the voltammograms. Analogous processes occurring for deposition/stripping from Pt nanoparticle-modified electrodes.

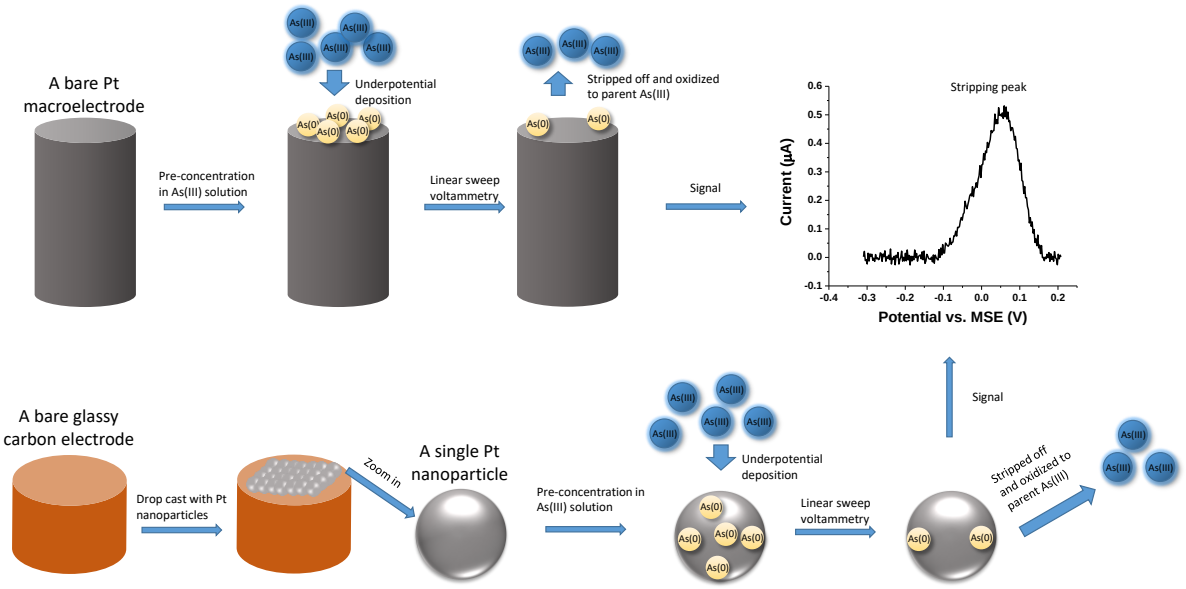

Scheme 1 A schematic diagram representing the underpotential deposition and anodic stripping voltammetry on a Pt macroelectrode (top) and a Pt nanoparticle (bottom).

Observations of As-related Peaks in ASV Figure 3a illustrates the linear sweep voltammetric response at a Pt macroelectrode in various concentrations of As(III) in 0.1 M H_2SO_4 after pre-concentration of As(0) and three arsenic-related peaks were observed as 5, 5' and 6. Peaks 5 and 6 were observed at ca -0.2 V and ca +0.4 V which corresponded to anodic stripping of bulk As(0) and oxidation of As(III) to As(V), respectively; the peak current of both peaks increased when the concentration of As(III) varies from 0 to 7.5 μM. Peak 5' at +0.05 V was assigned as the stripping peak associated with the oxidation

of As(0) ad-atoms [29a]. How the peak current of peak 5' varied with concentration of As(III) in solution at a Pt macroelectrode is plotted in Figure 3c. It is shown that the peak current of peak 5' increased with the concentration of As(III) and reached a plateau for As(III) concentrations higher than 2 µM. At higher concentrations the peak is obscured by the much larger peak 5. This observation sets the *upper* limit for detection with peak 5' at a Pt macroelectrode as 2 µM. A similar trend was observed by plotting the charge of peak 5' as a function of As(III) concentration as shown in Figure 3e. A limiting charge value of ca 9.4×10^{-7} C and a corresponding surface coverage of ca 1.7×10^{-10} mol cm^{-2} (see SI section 4 for calculation), are consistent with a sub-monolayer of As(0) ad-atoms deposited onto the surface of Pt.

The same experiment was conducted on a Pt nanoparticle-modified GCE. Figure 3b shows the linear sweep voltammetric response at the Pt nanoparticle-modified GCE in which contained approximately 0.1 monolayers of Pt nanoparticles (shown in the section 1 of SI). The voltammetric features observed (peaks 5, 5' and 6) are similar in potential and peak shape to that at Pt macroelectrode, which were at -0.2V, +0.05 V and +0.4V, respectively. Calbelka *et al* also reported the As ad-atoms oxidation peak at ca +0.01 V [29a], which was similar to our experimental result of peak 5' on both Pt macroelectrode and Pt nanoparticle-modified electrode. Accordingly the peak 5' was assigned as the stripping peak of deposited As(0) ad-atoms on surface of Pt. The plots illustrating how the peak current and charge of peak 5' varies as a function of As(III) concentration at a Pt nanoparticle-modified electrode are presented in Figure 3d and 3f, respectively. Similar to the bulk Pt, the peak current and charge increased approximately linearly from 0.05 to 2 µM and the slope started to decrease at 2 µM with a charge value of As deposited on the surface as ad-atoms of ca 9×10^{-7} C (ca 0.02 monolayers). The enhancement of signal in Figures 3d and 3f indicates that there were more available deposition sites at the surface of Pt nanoparticles than at bulk Pt for the coverages employed.

Table 2 shows the estimated coverage of As ad-atoms from the analysis of peak 5' of ASV at both Pt macroelectrode and Pt nanoparticle-modified GCE with the assumption that As ad-atoms were closely

packed on Pt surface. The geometric area was used for Pt macroelectrode while for Pt nanoparticle-modified electrode, the total area of Pt nanoparticles was used in the analysis. The number of Pt nanoparticles presented on the electrode surface was estimated to be ca 9×10^8 and each nanoparticle to have a surface area of 1.2×10^{-10} cm^2 assuming each particle to be a sphere of radius 15 nm with a roughness factor of 4.4 ± 1.1 [32]. Detailed calculations for Pt macroelectrodes and Pt nanoparticle-modified electrodes are shown in SI sections 4 and 5, respectively. The coverage and layers of As ad-atoms at bulk Pt were much higher than that at Pt nanoparticles, which was contributed by the larger surface area of the mesoporous Pt nanoparticles. The continuous increase towards a limiting value of the peak current (Figure 3d) and charge (Figure 3f) of peak 5' at Pt nanoparticle-modified electrode with concentrations of As(III) higher than 2 µM, is as expected for UPD with the limiting value approaching that of ca one monolayer. Based on the experimental results, under the conditions studied there were less than one monolayer of As ad-atoms deposited onto the surface of Pt even increasing the concentrations of As(III) or lengthening the deposition time. The analytical measurements in this study were thus based on the sub-monolayer of deposited As(0) ad-atoms.

Table 2. Analysis of peak 5' measured in 2 µM As(III) at a Pt macroelectrode and at a Pt nanoparticle-modified GCE. LSV parameters: deposition at -0.7 V vs. MSE for 240s, potential scan rate 0.1 V s^{-1}.

	Concentration (µM)	Charge (C)	Surface area of Pt (cm^2)	Number of moles of As (mol)	Coverage of As ad-atoms (mol cm^{-2})	Monolayers of As ad-atoms
Pt macroelectrode	2	9.4×10^{-7}	0.02	3.3×10^{-12}	1.7×10^{-10}	0.14
Pt nanoparticle-modified electrode	2	9×10^{-7}	0.11	3.2×10^{-12}	2.6×10^{-11}	0.02

Although linear responses of peaks 5 and 6 as a function of concentration of As(III) in the range 1 to 7.5 µM was observed (Figure S7 in the SI) and these two features are suitable as the basis for the analysis of As(III) as already extensively reported in the literature [15], peak 5 was observed to be difficult to be observed at concentrations lower than 2 µM (150 ppb) and peak 6 had a detection limit of 1 µM (75 ppb) at both bulk Pt and Pt nanoparticles (Figures 3a and 3b). These two detection limits

are much higher than the WHO limit for drinking water, 10 ppb. Further attention was thus focussed on the novel use of peak 5'.

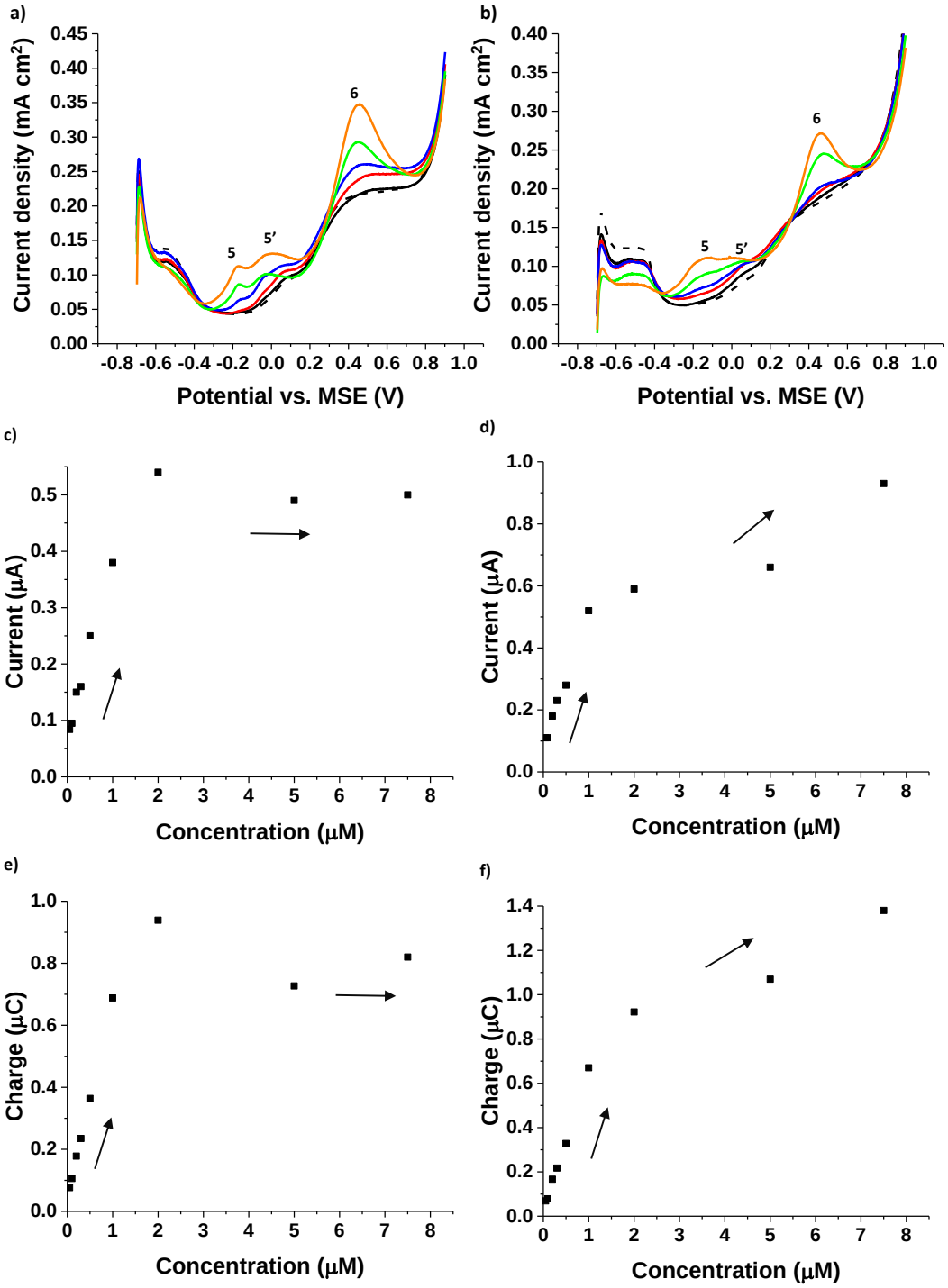

Figure 3. LSV curves of various concentrations of As(III) in 0.1 M H_2SO_4 at a) Pt macroelectrode and b) Pt nanoparticle-modified GC electrode. The concentrations of As(III) were 0 µM (black dash line), 0.5 µM (black solid line), 1 µM (red), 2 µM (blue), 5 µM (green) and 7.5 µM (orange). Peak current of peak 5' vs. concentrations of As(III) at c) Pt macroelectrode and d) Pt nanoparticle-modified GCE. Charge of peak 5' vs. concentrations of As(III) at e) Pt macroelectrode and f) Pt nanoparticles GCE. The numbers in c), d), e) and f) were calculated from baseline corrected LSVs. LSV parameters: deposition at -0.7 V vs. MSE for 240s, potential scan rate 0.1 V s^{-1}.

Calibration Curves and Limits of Detection Figures 4a and 4b show the baseline corrected LSV of peak 5' with various concentrations of As(III) in 0.1 M H_2SO_4 at Pt macroelectrode and Pt nanoparticle-modified electrode, respectively. The full procedure for the baseline corrections is reported in SI section 6. The LSVs were obtained with the same procedure as above. Concentrations of As(III) were studied between 0.05 µM and 1 µM, to avoid the interference from peak 5. The peak height and peak width were seen to increase with the concentration of As(III) at both electrodes, corresponding to more As(0) deposited. Note that the estimated covered area of the Pt nanoparticles on GCE was ca 0.008 cm^2 (calculations shown in section 1 of SI), which was much smaller than the geometric area of the Pt macroelectrode, 0.02 cm^2. However, the surface area of particles were much larger than geometric area of Pt macroelectrode due to the mesoporous structure and the roughness of surface. The large surface area of mesoporous Pt nanoparticles contributed more deposition sites for As(0), and thus more arsenic ad-atoms can be deposited onto the surface of Pt nanoparticles and generate a similar sized signal as seen at bulk Pt.

The stripping peak of the As(0) ad-atoms (peak 5') was investigated for analytical use. Calibration curves were made at both electrodes (Inset figures for Figures 4a and 4b), and the linear relationship was obtained from 0.05 µM to 1 µM. A LOD of 0.05 µM, 4 ppb, was obtained at both electrodes and the sensitivities of 6.4×10^{-7} C μM^{-1} and 6.3×10^{-7} C μM^{-1} were obtained on bulk Pt and Pt nanoparticle-modified electrodes, respectively. Note that the quoted LOD is estimated on the basis of the visual identification of measureable signals from real samples rather than calculated based on the 3σ method. Examples of the smallest signals deemed 'measureable' are given in the section 8 of SI.

The detection limit obtained using measureable, visually clear signals of 4 ppb meets the detection limits needed to implement the WHO guidelines for arsenic in drinking water (see Introduction). All these experiments were repeated 3 times and the variation was found to be less than 12% and 8% standard deviation at Pt macroelectrode and Pt nanoparticle-modified GCE, respectively.

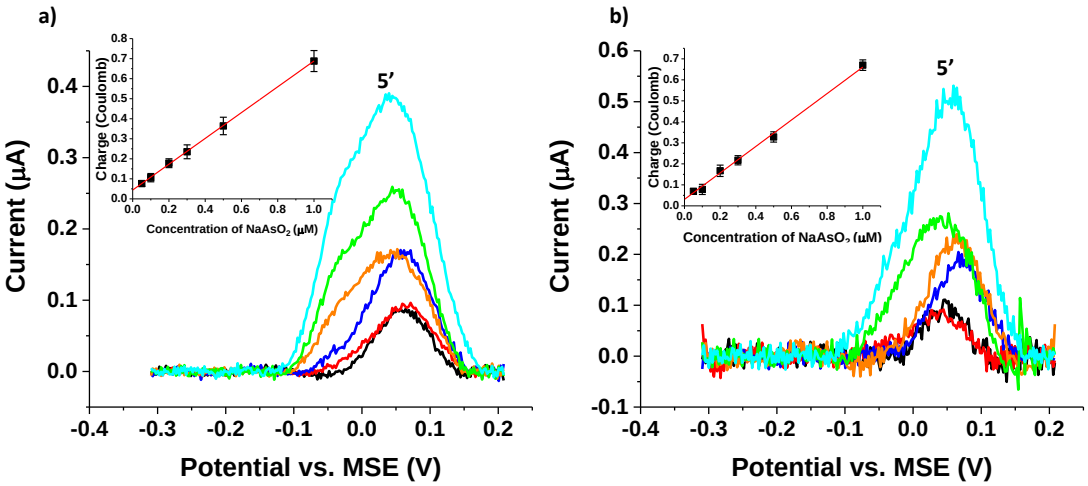

Figure 4. Baseline corrected LSV curves of various concentrations of As(III) in 0.1 M H_2SO_4 at a) Pt macroelectrode and b) Pt nanoparticle-modified GC electrode. The concentrations of As(III) were 0.05 µM (black), 0.1 µM (red), 0.2 µM (blue), 0.3 µM (orange), 0.5 µM (green) and 1 µM (cyan). Inset: Charge of stripped As(0) ad-atoms vs. the concentration of As(III). The charge was calculated from baseline corrected LSVs and error bars were standard deviations calculated from at least sets of data. LSV parameters: deposition at -0.7 V vs. MSE for 240s, potential scan rate 0.1 V s^{-1}, and baseline was modelled via polynomial method from -0.3 V to +0.2 V for peak 5'.

Interference studies

Having established an analytical procedure based on the stripping of As(0) ad-atoms from Platinum surface, further experiments were conducted to explore if the possible presence of either Cu(II) or chloride ions interfered with the measurements.

Possible interference of Cu(II)

Cu(II) is a very commonly encountered interferent in stripping voltammetry of As since Cu forms alloys and intermetallic compounds with bulk As(0) [18]. Accordingly the interference of Cu(II) with detection of low concentrations of As(III) was studied using ASV by adding different amounts of Cu(II) in the solution. Figure 5a illustrates the baseline corrected LSV of 0.5 µM As(III) in 0.1 M H_2SO_4 with additions of Cu(II) (0.5 µM each time) at Pt macroelectrode with a potential range of -0.3 V to + 0.2 V. The black dashed line was recorded for a solution without Cu(II) where only one peak was observed at ca +0.05V corresponding to the oxidation of As ad-atoms [29a]. With the addition of Cu(II), the signal of peak 5' varied negligibly and the peak potential did not shift. It can be therefore concluded that Cu(II) did not interfere to the oxidation peak of As ad-atoms. Similarly, Figure 5b shows the baseline corrected LSV

of 0.5 µM As(III) in 0.1 M H_2SO_4 with additions of Cu(II) (0.5 µM each time) at Pt nanoparticle-modified GCE. Again the addition of Cu(II) did not change the signal of peak 5' or shift the potential of it by comparing the voltammograms obtained without (black dashed line in Figure 5b) and with Cu(II). We conclude that the formation of Cu-As alloys or intermetallic species was avoided by using As ad-atoms as the indicator.

We further considered the electrodeposition of Cu from high concentrations of Cu(II). The ASVs of 50 µM As(III) in 0.1 M H_2SO_4 with additions of Cu(II) (50 µM each) at bulk Pt and Pt nanoparticles are shown in Figure S9 in SI. It is shown that only the concentration of Cu(II) reached 50 µM or higher, the Cu peak at ca -0.4 V interfered with peak 5 and begins to overlap with peak 5' (Figure S9). The method is therefore robust against copper interference except at extremely high concentration where dilution might be used to circumvent the problem.

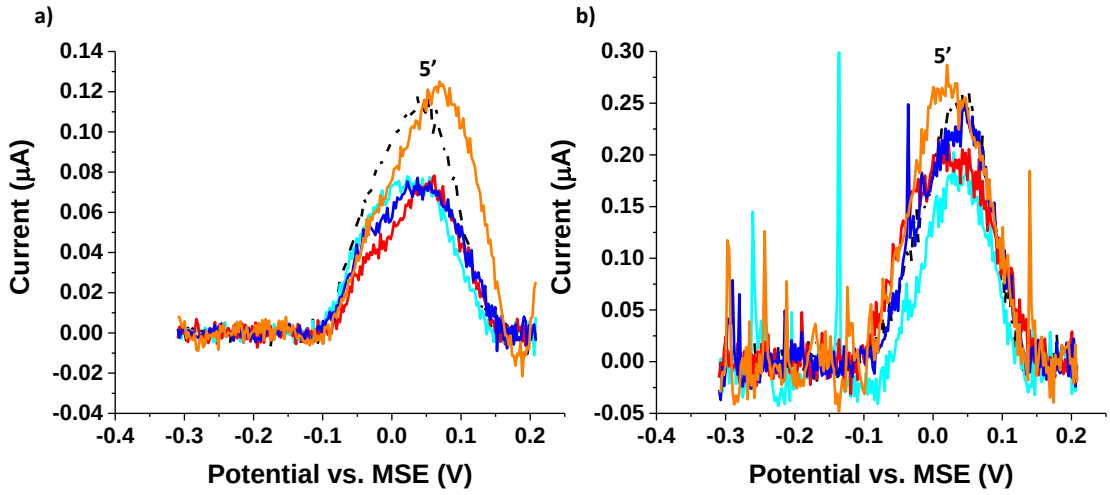

Figure 5. Baseline corrected LSV curves of Cu(II) additions (0.5 µM each) to 0.5 µM As(III) in 0.1 M H_2SO_4 in the potential range from -0.3 V to +0.2 V at a) Pt macroelectrode and b) Pt nanoparticle-modified GC electrode. LSV parameters: deposition at -0.7 V for 240s, scan rate was 0.1 V s^{-1}. Cu(II) concentration: 0 µM (black dash line), 0.5 µM (cyan), 1 µM (red), 1.5 µM (blue) and 2 µM (orange).

Possible interference of chloride

Chloride is known to be adsorbed onto Pt surfaces [35]. The peak of Pt to Pt oxide in 0.1M H_2SO_4 is reported to be shifted to more positive potentials with the addition of 10 µM Cl^- [35]. Meanwhile, the reduction peak of the Pt oxide shifted to less negative potentials. The peak current of oxide formation

did not change while the peak current of the oxide removal was reduced with the addition of chloride. Pempegowda *et al* applied graphene-Pt nanoparticle-modified GCE for As(III) detection with SWASV where chloride was reported as an interferent but only at concentrations above 450 μM [20b]. Therefore, the possible interference of chloride under low As(III) concentrations conditions was considered and investigated using ASV in this section.

Figure 6a displays the baseline corrected LSVs of 0.5 μM As(III) in 0.1 M H_2SO_4 in the presence of 0.5 (cyan), 1 (red), 1.5 (blue) and 2 μM (orange) chloride at a Pt macroelectrode with a potential range of -0.3 V to +0.2 V. Pre-concentration of As(0) ad-atoms was carried out at -0.7 V for 240 s and LSV was subsequently conducted from -0.7 V to +0.9 V at a scan rate of 0.1 V s^{-1}. With the addition of chloride, the signal of peak 5' at ca +0.05 V did not change in both peak current and peak potential indicating negligible interference of chloride at these concentrations. The response at higher concentrations is shown in Figure 6c for 50 μM As(III) in 0.1 M H_2SO_4 in the presence of 50 (cyan), 100 (red), 150 (blue) and 200 μM (orange) chloride at a Pt macroelectrode. Three peaks labelled as peaks 5, 5' and 6 were observed at ca -0.25 V, ca +0.05 V and ca +0.4 V, which were ascribed to the oxidation of bulk As(0), oxidation of As ad-atoms and oxidation of As(III) to As(V), respectively [15, 29a]. The black dashed line was recorded for a solution without chloride. It is obvious that the chloride did not interfere with peaks 5 and 6 as literature presented [20b]. The signal of peak 5' was reduced suggesting an upper limit of ca 100 μM above which the analytical use of the peak is not possible probably due to competitive adsorption between As and chloride. Similar limits were observed at Pt nanoparticle-modified electrodes (see figures 6b and 6d). The sensitivity to chloride imposes limitations for the range of samples amenable to analysis via the proposed method [36].

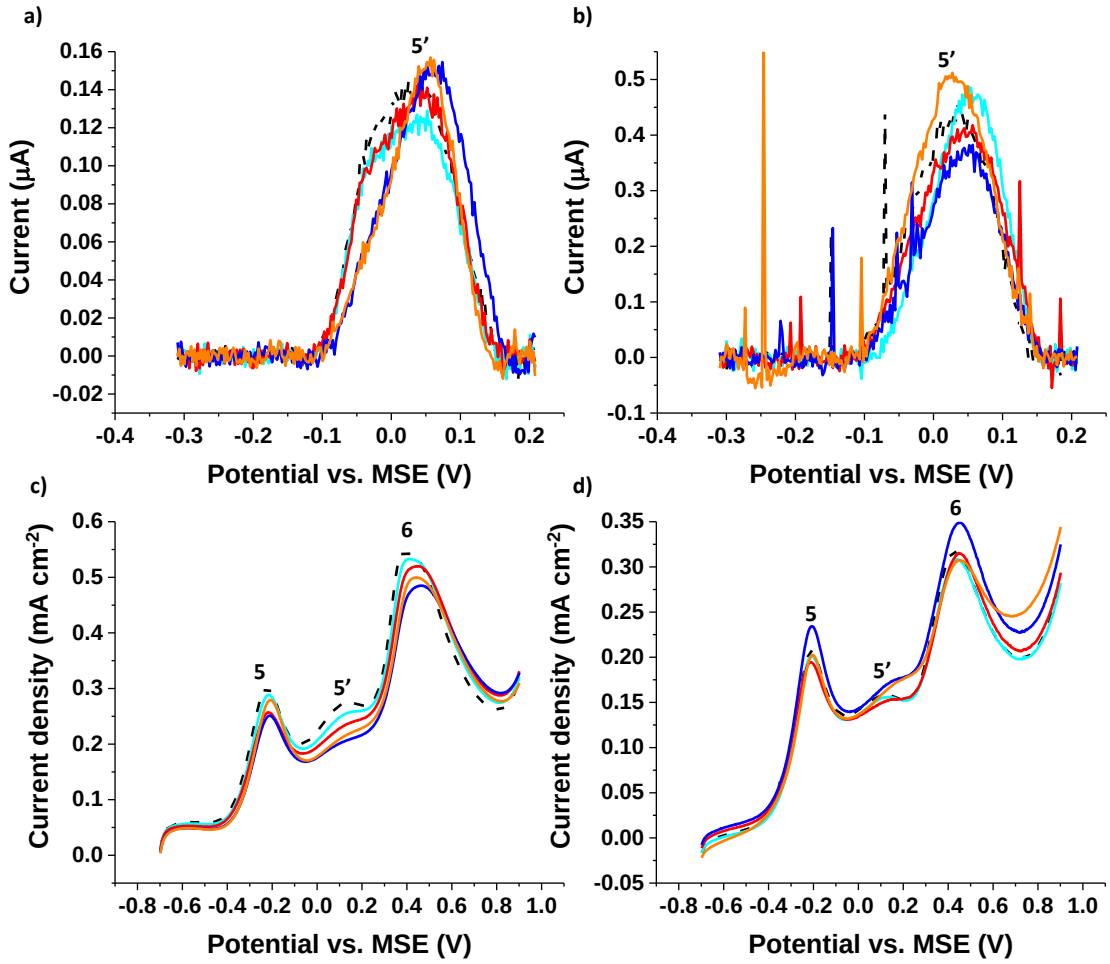

Figure 6. Baseline corrected LSV curves of Cl^- additions (0.5 µM each) to 0.5 µM As(III) in 0.1 M H_2SO_4 in the potential range from -0.3 V to +0.2 V at a) Pt macroelectrode and b) Pt nanoparticle-modified GCE. Cl^- concentration: 0 µM (black dash line), 0.5 µM (cyan), 1 µM (red), 1.5 µM (blue) and 2 µM (orange). LSV curves of Cl^- additions (50 µM each) to 50 µM As(III) in 0.1 M H_2SO_4 in the potential range from -0.7 V to +0.9 V at c) Pt macroelectrode and d) Pt nanoparticle-modified GC electrode. Cl^- concentrations: 0 µM (black dash line), 50 µM (cyan), 100 µM (red), 150 µM (blue) and 200 µM (orange). LSV parameters: deposition at -0.7 V for 240s, scan rate was 0.1 V s^{-1}.

Conclusions

The possible analytical use of under-potential deposition of As on platinum surface combined with anodic stripping of the adsorbed As atoms has been explored using both platinum macro-electrodes and platinum nanoparticle-modified electrodes. A limit of detection within the requirements imposed by the WHO guidelines for safe drinking water was observed with the significant merit that the determinations were free from interference by Cu(II) which often blights the use of ASV when bulk As is deposited. On the other hand the method was sensitive to the presence of chloride which likely

limits the analytical application to largely chloride free media, for example to bottled mineral waters. No particular relative merits of using nanoparticle-modified electrodes over platinum macro-electrodes were observed with similar limits of detection measured.

References

[1] aX. C. Xu, X. H. Niu, X. Li, Z. H. Li, D. Du, Y. H. Lin, *Sens. Actuator B-Chem.* **2020**, *315*, 13; bS. Sikdar, M. Kundu, *ChemBioEng Rev.* **2018**, *5*, 18-29; cA. S. Maghsoudi, S. Hassani, K. Mirnia, M. Abdollahi, *Int. J. Nanomed.* **2021**, *16*, 803-832; dX. P. Yu, C. L. Liu, Y. F. Guo, T. L. Deng, *Molecules* **2019**, *24*, 23; eS. Li, C. Zhang, S. Wang, Q. Liu, H. Feng, X. Ma, J. Guo, *Analyst* **2018**, *143*, 4230-4246.

[2] P. Boffetta, C. Borron, *Dose-Response* **2019**, *17*, 1559325819863634.

[3] WHO, in *WHO chronicle, Vol. 38*, **2011**, pp. 104-108.

[4] aJ. M. Hao, M. J. Han, S. M. Han, X. G. Meng, T. L. Su, Q. W. K. Wang, *J. Environ. Sci.* **2015**, *36*, 152-162; bM. Welna, A. Szymczycha-Madeja, P. Pohl, *Trac-Trends Anal. Chem.* **2015**, *65*, 122-136; cM.-L. Chen, L.-Y. Ma, X.-W. Chen, *Talanta* **2014**, *125*, 78-86.

[5] G. M. dos Santos, D. Pozebon, C. Cerveira, D. P. de Moraes, *Microchem. J.* **2017**, *133*, 265-271.

[6] aI. Komorowicz, A. Hanć, W. Lorenc, D. Barałkiewicz, J. Falandysz, Y. Wang, *Chemosphere* **2019**, *233*, 223-233; bY.-L. Feng, H.-Y. Chen, L.-C. Tian, H. Narasaki, *Anal. Chim. Acta* **1998**, *375*, 167-175.

[7] H. Cheng, W. Zhang, Y. Wang, J. Liu, *Microchim. Acta* **2018**, *185*, 1-8.

[8] aF. W. Campbell, R. G. Compton, *Anal. Bioanal. Chem.* **2010**, *396*, 241-259; bM. B. Gumpu, S. Sethuraman, U. M. Krishnan, J. B. B. Rayappan, *Sens. Actuator B-Chem.* **2015**, *213*, 515-533; cB. Bansod, T. Kumar, R. Thakur, S. Rana, I. Singh, *Biosens. Bioelectron.* **2017**, *94*, 443-455.

[9] aJ. Wang, *Stripping analysis: principles, instrumentation, and applications*, Vch Pub, **1985**; bK. Brainina, E. Neyman, *Electroanalytical stripping methods, Vol. 185*, John Wiley & Sons, **1994**; cJ. Wang, *Environ. Sci. Technol.* **1982**, *16*, 104A-109A.

[10] L. Xiao, G. G. Wildgoose, R. G. Compton, *Anal. Chim. Acta* **2008**, *620*, 44-49.

[11] K. Pungjunun, S. Chaiyo, I. Jantrahong, S. Nantaphol, W. Siangproh, O. Chailapakul, *Microchim. Acta* **2018**, *185*, 1-8.

[12] E. Fischer, C. M. van den Berg, *Anal. Chim. Acta* **1999**, *385*, 273-280.

[13] A. O. Simm, C. E. Banks, R. G. Compton, *Electroynalysis (N.Y.N.Y.)* **2005**, *17*, 1727-1733.

[14] L. Bu, T. Gu, Y. Ma, C. Chen, Y. Tan, Q. Xie, S. Yao, *J. Phys. Chem. C* **2015**, *119*, 11400-11409.

[15] X. Dai, R. G. Compton, *Analyst* **2006**, *131*, 516-521.

[16] A. Profumo, D. Merli, M. Pesavento, *Anal. Chim. Acta* **2005**, *539*, 245-250.

[17] D. Jedryczko, P. Pohl, M. Welna, *Talanta* **2016**, *150*, 265-271.

[18] A. Idris, J. Mafa, N. Mabuba, O. Arotiba, *Electrochem. Commun.* **2016**, *64*, 18-20.

[19] aW. Chen, H. Yu, S.-Y. Lee, T. Wei, J. Li, Z. Fan, *Chem. Soc. Rev.* **2018**, *47*, 2837-2872; bR. Miao, L. Chen, L. Shao, B. Zhang, R. G. Compton, *Angew. Chem., Int. Ed.* **2019**, *58*, 12549-12552; cM. Pumera, *Chem. Soc. Rev.* **2010**, *39*, 4146-4157; dX. Li, C. Batchelor‐McAuley, S. A. Whitby, K. Tschulik, L. Shao, R. G. Compton, *Angew. Chem., Int. Ed.* **2016**, *55*, 4296-4299.

[20] aD. D. Han, Z. G. Liu, J. H. Liu, X. J. Huang, *RSC Adv.* **2015**, *5*, 38290-38297; bR. Kempegowda, D. Antony, P. Malingappa, *Int J Smart Nano Mater* **2014**, *5*, 17-32; cW. B. Postek, I. A. Rutkowska, J. A. Cox, P. J. Kulesza, *Electrochim. Acta* **2019**, *319*, 499-510.

[21] aY. Zhang, A. K. Selva Kumar, D. Li, M. Yang, R. G. Compton, *ChemElectroChem* **2020**, *7*, 4614-4624; bT. J. Davies, R. R. Moore, C. E. Banks, R. G. Compton, *J. Electroanal. Chem.* **2004**, *574*, 123-152.

[22] K. R. Ward, M. Gara, N. S. Lawrence, R. S. Hartshorne, R. G. Compton, *J. Electroanal. Chem.* **2013**, *695*, 1-9.
[23] H. Xu, L. Zeng, S. Xing, Y. Xian, L. Jin, *Electrochem. Commun.* **2008**, *10*, 551-554.
[24] J.-F. Huang, H.-H. Chen, *Talanta* **2013**, *116*, 852-859.
[25] M. Yang, X. Chen, J. H. Liu, X. J. Huang, *Sens. Actuator B-Chem.* **2016**, *234*, 404-411.
[26] aJ. A. Rodrigues, C. M. Rodrigues, P. J. Almeida, I. M. Valente, L. M. Gonçalves, R. G. Compton, A. A. Barros, *Anal. Chim. Acta* **2011**, *701*, 152-156; bJ. Orozco, C. Fernandez-Sanchez, C. Jimenez-Jorquera, *Environ. Sci. Technol.* **2008**, *42*, 4877-4882.
[27] aC. A. Paddon, R. G. Compton, *J. Phys. Chem. C* **2007**, *111*, 9016-9018; bO. A. Oviedo, L. Reinaudi, S. G. García, E. P. M. Leiva, *Monographs in Electrochemistry* **2016**; cE. Herrero, L. J. Buller, H. D. Abruña, *Chem. Rev.* **2001**, *101*, 1897-1930.
[28] B. Y. Ren, L. A. Jones, M. Chen, D. K. Oppedisano, D. Qiu, S. J. Ippolito, S. K. Bhargava, *J. Electrochem. Soc.* **2017**, *164*, H1121-H1128.
[29] aT. D. Cabelka, D. S. Austin, D. C. Johnson, *J. Electrochem. Soc.* **1984**, *131*, 1595; bW. Zhou, L. Kibler, D. Kolb, *Electrochim. Acta* **2004**, *49*, 5007-5012; cJ. Feliu, A. Fernandez-Vega, A. Aldaz, J. Clavilier, *J. Electroanal. Chem. Interf. Electrochem.* **1988**, *256*, 149-163.
[30] aM. Yang, P. H. Li, W. H. Xu, Y. Wei, L. N. Li, Y. Y. Huang, Y. F. Sun, X. Chen, J. H. Liu, X. J. Huang, *Sens. Actuator B-Chem.* **2018**, *255*, 226-234; bB. M. Sonkoue, P. M. S. Tchekwagep, C. P. Nanseu-Njiki, E. Ngameni, *Electroanalysis* **2018**, *30*, 2738-2743; cJ. H. Hwang, P. Pathak, X. C. Wang, K. L. Rodriguez, J. Park, H. J. Cho, W. H. Lee, *Sens. Actuator B-Chem.* **2019**, *294*, 89-97; dC. Nunez, J. J. Trivino, R. Segura, V. Arancibia, *Microchem. J.* **2020**, *159*, 6.
[31] G. Bhanjana, N. Dilbaghi, S. Chaudhary, K. H. Kim, S. Kumar, *Analyst* **2016**, *141*, 4211-4218.
[32] W. Yu, C. Batchelor-McAuley, X. Chang, N. P. Young, R. G. Compton, *Phys Chem Chem Phys* **2019**, *21*, 20415-20421.
[33] A. K. S. Kumar, Y. Zhang, D. Li, R. G. Compton, *Electrochem. Commun.* **2020**, 106867.
[34] Y. Zhang, A. K. S. Kumar, D. Li, M. Yang, R. G. Compton, *ChemElectroChem* **2020**.
[35] D. M. Novak, B. E. Conway, *J. Chem. Soc. Faraday Trans.* **1981**, *77*, 2341-2359.
[36] W. H. Organization, (Ed.: W. H. Organization), Geneva, **2003**.

Table of contents:

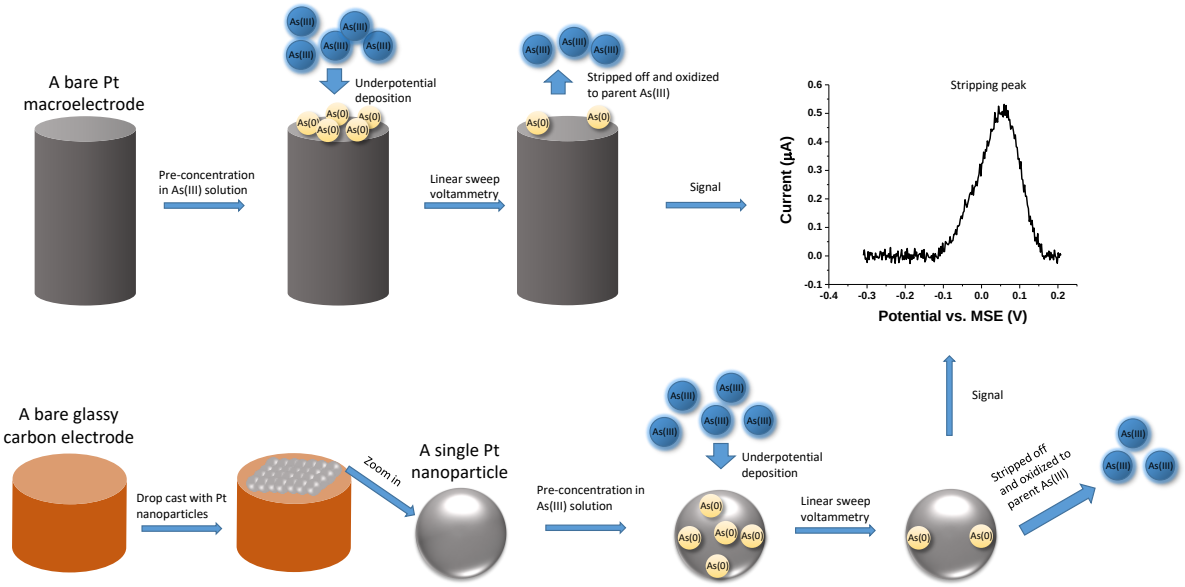

A schematic diagram representing the underpotential deposition and anodic stripping voltammetry of As on a Pt macroelectrode or a Pt nanoparticle modified electrode.